Disorder Originated Unusual Mobility in Crystalline $InGaZnO_4$

Yoon Jegal, Adem H. Kulahlioglu, Chang-Ki Baek, *Senior Member, IEEE*, and Byoung Don Kong, *Member, IEEE*

***Abstract*— Using calculations from first principles, the site disorder between Ga and Zn of crystalline $InGaZnO_4$ is shown to play key roles in its unique transport properties. The analysis based on Density Functional Theory reveals that the various types of scattering centers stem from the charge imbalance between the ordered and disordered structures are the prime factor in explaining the carrier mobility of the crystalline $InGaZnO_4$. The phonon dispersion of crystalline $InGaZnO_4$ is also examined to include the influence of scattering by polar optical phonons. The Hall mobility calculation based on Boltzmann transport equation under relaxation time approximation shows that the site disorders of $2.5\times10^{21}cm^{-3}\sim5\times10^{21}cm^{-3}$ can dominate the transport character. The comparisons with experimental data demonstrate excellent agreement in the wide ranges of temperature (100 ~ 300 K) and doping densities (10^{16} ~ 10^{20} cm^{-3}). Our results provide a critical measure to estimate a device performance utilizing quasi-crystalline $InGaZnO_4$ along with a deeper understanding of its peculiar transport characters.**

***Index Terms*— $InGaZnO_4$ (IGZO), disorder, transport, mobility, density functional theory.**

I. Introduction

INDIUM Gallium Zinc Oxide (IGZO) is a pivotal material for display applications. The relatively high mobility in its amorphous phase (a-IGZO) has made it ideally suited for a channel material of thin-film transistors (TFTs) [1], [2]. The a-IGZO TFTs have rapidly replaced the traditional a-Si TFTs, leading the cutting-edge display technologies [1]. The recent synthesis of C-Axis Aligned Crystalline $InGaZnO_4$ (CAAC-IGZO) [3], [4] has suggested a richer potential of the material for previously unexpected areas such as Large-Scale Integrated circuits (LSI) [5] or Memory [6]. The CAAC-IGZO films, grown by cost-effective sputtering [7], has a *c*-axis alignment similar to that of a single crystal, while the *a*-*b* plane shows mosaic patterns without grain boundaries, which is clearly distinct from an amorphous or a polycrystalline phase [4]. This quasi-crystalline phase of IGZO has demonstrated high stability [8] and low off-leakage current [9] that bring the material up as a candidate to replace a-Si or poly-Si in logic applications. Yet the transport properties of the IGZO is less studied [10]–[12]. In [10], [11], the unusual mobility behavior of IGZO, increasing with a higher carrier density, was explained by the fluctuation of the conduction band minima (CBM) originated from the random distribution of Ga and Zn. It was claimed that the fluctuation of band could be seen as potential barriers, and with higher Fermi level, electrons might surpass the barrier easily. However, this is rather phenomenological explanation that does not include any scattering mechanism. In [12], more rigorously an alloy scattering model, typically used for IV or III-V compounds such as Si_xGe_{1-x}, was applied, but the calculated mobility has an order of magnitude difference with recent measurements [13]. For the applications aiming at a few nanometer technology node such as LSI and Memory, a more accurate description of the carrier transport becomes mandatory.

In this letter, we report the first principles' analysis of the carrier transport of crystalline IGZO (c-IGZO). Based on the examination of the impact of the disorders using Density Functional Theory (DFT), Hall mobility in a wide range of carrier densities and temperatures were calculated using the relaxation time approximation (RTA) of the Boltzmann transport equation (BTE) to provide a consolidated picture of the carrier transport in IGZO at various operating conditions.

II. Disorder Modeling and Mobility Calculations

Zn and Ga, placed next to each other in the periodic table, can easily substitute each other in c-IGZO, creating site disorders. The disorders were modeled using QUANTUM-ESPRESSO DFT suite [14]. Norm-conserving pseudo-potentials [15] under the generalized gradient approximation (GGA) were used with a plane wave expansion up to 80 Ry. $6 \times 6 \times 4$ Monkhorst-Pack grids were adopted for the Brillouin zone (BZ) sampling. The c-IGZO cells were represented by a hexagonal lattice with 21 basis atoms [3]. The influence of site disorders was investigated by examining the changes in physical properties from the minimum energy atomic configuration, i.e., the ordered structure. The ordered structure was found to be the atomic sequence of In-Zn-Ga (omitting O) which was shown in Fig. 1 (a) left. An example of the site disorder – when Ga and Zn are switched in the middle – are shown in Fig. 1 (a) right. The crystal energy

Manuscript received April 1, 2020; accepted April 11, 2020. Date of publication April 20, 2020; date of current version May 21, 2020. This work was supported in part by Samsung Electronics Company Ltd., via Samsung-POSTECH Industrial Academic Cooperation Program. The review of this letter was arranged by Editor V. Moroz. *(Corresponding author: Byoung Don Kong.)*

Yoon Jegal, Adem H. Kulahlioglu, and Byoung Don Kong are with the Department of Electrical Engineering, Pohang University of Science and Technology, Pohang 37673, South Korea (e-mail: bdkong@postech.ac.kr).

Chang-Ki Baek is with the Department of Creative IT Engineering, Pohang University of Science and Technology, Pohang 37673, South Korea.

Color versions of one or more of the figures in this letter are available online at http://ieeexplore.ieee.org.

Digital Object Identifier 10.1109/LED.2020.2988674

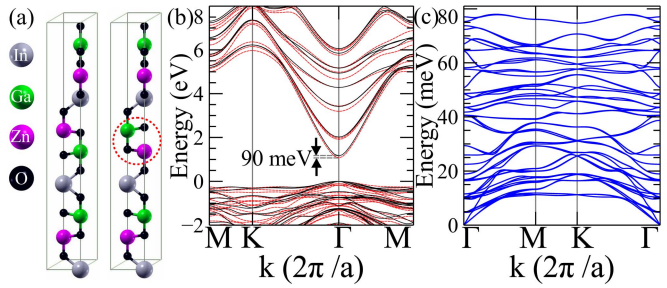

Fig. 1. Crystal structure of c-IGZO, energy band, and phonon dispersion. (a) Left: ordered structure. Right: disordered structure. (b) Band structure of the ordered (black solid) and the disordered (red dashed) c-IGZO. (c) Phonon dispersion of c-IGZO.

difference between the ordered and disordered structures was 8.16 meV, while the lattice constants for both systems are almost identical ($a = 3.36$ Å and $c = 26.1$ Å). All structures were relaxed until the inter-atomic forces decreased below 0.015eV/Å. Thus, the site disorders can easily occur without influencing the crystal volume. Fig. 1 (b) illustrates the band structure change, showing that the influence of the disorder on the electronic energy bands is very limited: 90 meV shift in the conduction band (CB), and this shows the application of the fluctuating CBM model is also limited. The calculated effective mass (m) of the CB was $0.25m_e$, where m_e is the electron rest mass, which is in good agreement with previous studies [3], [12]. To include the influence of phonons [16], [17], the phonon dispersion was calculated using the density functional perturbation theory (DFPT) [18]. The calculated dispersion along the symmetry points is shown in Fig. 1 (c).

While the band structure variation is minimal, there must be a charge shift when a Zn and a Ga are switched since the nuclei charges are different. In addition, the atomic bondings can be changed. To explore this possibility, a $3 \times 3 \times 1$ supercell was constructed. A local disorder was introduced at the center of the supercell, and the differences in electron charge density and local ionic potential after the disorder occurred were calculated. In Fig. 2 (a), red and blue represent the positive and negative of the difference in local ionic potential, and Fig. 2 (b) shows the difference in electron density variations ($\Delta\rho$). In the magnified view (Fig. 2(c)), two types of $\Delta\rho$ can be found: one with an isolated single polarization (Ga and Zn sites), and the other with two adjacent opposite polarizations (nearby O sites) marked by yellow circles. It appears that the introduced disorder changes atomic configurations very little and induces only the charge deviation as shown in Fig. 2(c). In addition, the charge deviation is confined near the disorder site. Thus, the disorders can be considered independently. However, if the disorders are dense enough to change the atomic configurations substantially, such cases should be considered by separate DFT calculations. Disorder-induced $\Delta\rho$ creates monopolar and dipolar scattering centers. $\Delta\rho$ of monopoles (MPs) was $0.268e$ where e is the unit charge. The average $\Delta\rho$ and dipolar distance (d_o) of dipoles (DPs) were $0.456e$ and 0.8 Å. A site disorder whose nuclei charge difference is only $1e$ induces about nine scattering centers. This implies that the disorder-induced $\Delta\rho$ can play a critical role in carrier transport of c-IGZO. The effect was investigated by calculating Hall mobility and comparing the results with the experimental data.

For Hall mobility (μ_{Tot}), scattering by disorder MPs and DPs, ionized impurities (IIs) from the dopants, and polar optical phonons (POPs) were considered. The MPs and DPs can be considered separately. The physical origin of MP and II scatterings are identical except for the effective charge, and they can be treated together. The momentum relaxation time (MRT) by the II and MPs is given as [17]

$$\tau_{II-MP} = \frac{16\sqrt{2m}\pi\kappa_s^2\varepsilon_0^2}{\left(N_I + 2N_{Dis}\Delta Z_{Mono}^2\right)e^4} \times \left[\ln\left(1+\gamma^2\right) - \gamma^2\Big/\left(1+\gamma^2\right)\right]^{-1} E^{3/2}, \quad (1)$$

where $\gamma^2 \equiv 8mEL_D^2/\hbar^2$. $\kappa_s(=9.83)$ [19] is the static dielectric constant, and ε_0 is the vacuum permittivity. N_I and N_{Dis} are the impurity and disorder densities, respectively. Factor two in front of N_{Dis} is to account for positive and negative MPs per each disorder. E is electron energy. $L_D = \sqrt{F_{1/2}(\eta_C)\varepsilon_0\kappa_s k_B T/e^2 n F_{-1/2}(\eta_C)}$ [17] is the screening length, where T and n are the temperatures and the carrier densities. k_B stands for the Boltzmann constant, and $\hbar$ for the Planck constant. $F_j(x)$ is the Fermi integral with $\eta_C = (E_F - E_c)/k_B T$, where E_F and E_c are Fermi energy level and the CB minimum, respectively. The MRT of the DP [16] scattering reads as

$$\tau_{DP} = \frac{3 \times 2^{3/2}\pi\kappa_s^2\varepsilon_0^2\hbar^2\sqrt{E}}{e^4\sqrt{m}(\Delta Z_{dipole}d_o)^2 \times 7N_{dis}}, \quad (2)$$

where N_{Dis} is multiplied by seven to account for the number of DPs per each disorder. As for the scattering by phonons, only POP scattering is considered since μ of c-IGZO is less than $100cm^2/V\cdot s$. The acoustic phonon becomes negligible in this regime since the relaxation time by the acoustic phonon is at least one order of magnitude longer. Only longitudinal optical (LO) phonons have non-zero electron-phonon interaction coefficients under normal process [16], [20], and the first-order polarization of LO phonons arises by the contrary motion of the adjacent atoms in the primitive unit cell. In Fig. 1 (c), the mode satisfying this condition has the energy (E_p) of 73.77 meV. The MRT of the POP scattering [17] is given as

$$\tau_{POP} = \left\{\frac{e^2\omega_o\left(\kappa_s/\kappa_\infty - 1\right)}{4\pi\kappa_s\varepsilon_0\hbar\sqrt{2E/m}}\left[N_o\sqrt{1+\hbar\omega_o/E} + (N_o+1)\sqrt{1-\hbar\omega_o/E} - \frac{\hbar\omega_o N_o}{E}\sinh^{-1}\left(\hbar\omega_o/E\right)^{\frac{1}{2}} + \frac{\hbar\omega_o\left(N_o+1\right)}{E}\sinh^{-1}\left(E/\hbar\omega_o - 1\right)^{\frac{1}{2}}\right]\right\}^{-1}, \quad (3)$$

where $\kappa_\infty(=4.14)$ [19] is the high frequency dielectric constant and N_o is the optical phonon population. In the above equations, the screening effect is included in II scattering, while it is not considered for DP and POP scatterings. This is because, in II scattering, electrons can screen fixed ion since charge polarities are opposite, while DP and POP are deviations from normal electron distribution and electron cannot be screened by itself [16]. $\langle\tau\rangle \equiv \int_0^\infty \tau E^{3/2} f dE \Big/ \int_0^\infty E^{3/2} f dE$, where f is the Fermi-Dirac distribution. The Hall factors were

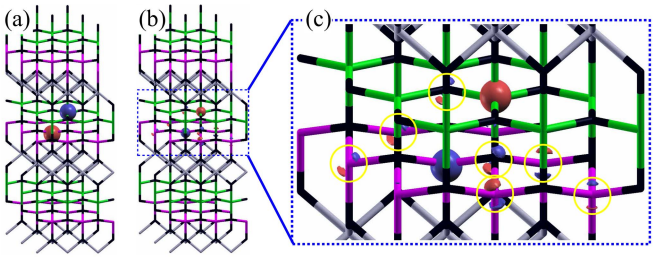

Fig. 2. Difference in local ionic potentials and electron charge densities of 3×3×1 supercell. (a) Difference local ionic potential between ordered and disordered supercell. (b) Difference in electron charge densities between ordered and disordered supercells. (c) Magnified view of (b).

obtained by evaluating $r_H = \langle\tau^2\rangle/\langle\tau\rangle^2$ [17]. The mobility per each scattering was calculated by $\mu = e\langle\tau\rangle r_H/m$, and by Matthiessen's rule, ${\mu_{Tot}}^{-1} = {\mu_{II}}^{-1} + {\mu_{POP}}^{-1} + {\mu_{Dip}}^{-1}$.

III. Results and Discussions

Fig. 3 summarizes the calculated mobility. Fig. 3 (a) display the comparison between calculated μ_{Tot} with different disorder densities and measurement data from [13] at $T = 300$ K. The most plausible comparisons were observed when $2.5\times10^{21}cm^{-3} \leq N_{Dis} \leq 5\times10^{21}cm^{-3}$. Fig. 3 (b) and (c) show the μ_{Tot} with N_{Dis} of $2.5\times10^{21}cm^{-3}$ and $5\times10^{21}cm^{-3}$, respectively, as a function of n and T. The disorder density $2.5\times10^{21}cm^{-3}$ i.e., Fig. 3 (b), gives the best agreement at n less than $1\times10^{19}cm^{-3}$, while the disorder density $5\times10^{21}cm^{-3}$ i.e., Fig. 3 (c), does the same at n greater than $1\times10^{19}cm^{-3}$. The experimental data in the same scale are provided in Fig. 3 (f) [13]. It should be pointed out that the experimental data are collected from many samples with different growth conditions, and N_{Dis} can vary depending on the samples. In this case, a point-by-point exact match with all the collected experimental data with a single N_{Dis} is practically impossible. However, the proposed model reproduces important features such as temperature and carrier density dependence with reasonable numerical accuracies. Essentially, N_{Dis} shifts the overall mobility levels (compare Fig. 3 (b) and (c)) and can be adjusted for a better fit to a specific curve. Nearly T-independent lines were found with $n \sim 2.5\times10^{18}cm^{-3}$ in our calculation (dashed lines) that can explain the experimental results with $n \sim 1\times10^{19}cm^{-3}$. The above analysis shows a general trend: the increased doping (higher n) can induce more site disorders. Since the atomic density of Ga or Zn is $1.18\times10^{22}cm^{-3}$, the calculated N_{Dis} suggests more ordered sites than disordered, which is possible since that is energetically preferred when the total crystal volume is considered, even though the energy difference between the unit cells is tiny.

Without the DP contribution, a good agreement with the T dependences of the experimental data over wide ranges of n and T is hard to be achieved. The T dependence of μ_{Tot} without dipole (Fig. 3 (d)) becomes strong at high n, unlike the experimental data.

Usual semiconductors show mobility drops at higher doping levels due to the increased II scattering, but c-IGZO shows the opposite trend. The disorder-induced scattering can explain this n-dependence. At low n, N_I is much smaller than $2N_{Dis}\Delta Z^2_{Mono}$, the disorder-induced MPs. However, N_I is the

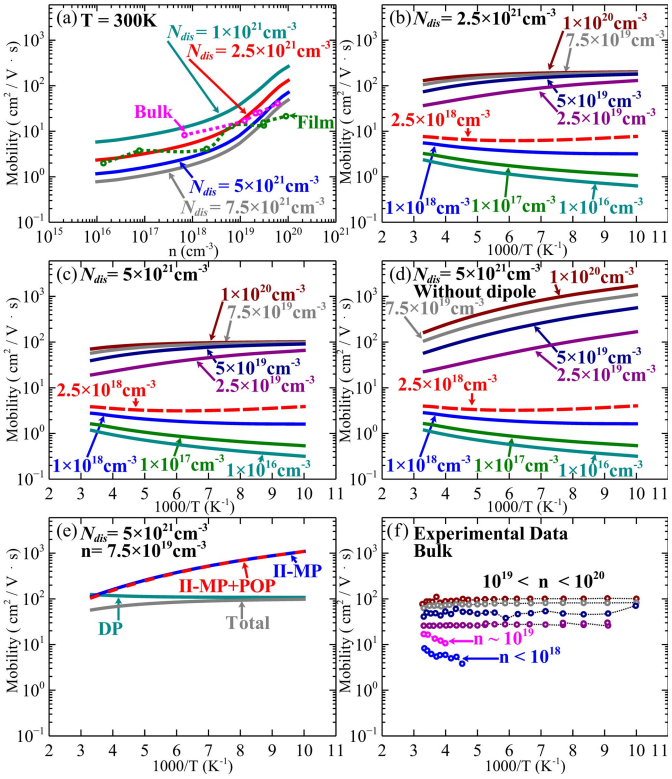

Fig. 3. Calculated mobility and comparison to experimental data. (a) Comparisons between calculated mobilities with different disorder densities. (b) Calculated μ_{Tot} with $N_{dis} = 2.5\times10^{21}cm^{-3}$. (c) Calculated μ_{Tot} with $N_{dis} = 5\times10^{21}cm^{-3}$. (d) Calculated μ_{Tot} without dipole contribution. $N_{dis} = 5\times10^{21}cm^{-3}$. (e) Each scattering contribution for $n = 5\times10^{19}cm^{-3}$ and $N_{dis} = 5\times10^{21}cm^{-3}$. μ_{POP} does not appear because it is out of scale. (f) Experimentally measured bulk μ from [13] for comparisons.

determining factor of the screening length. As N_I increases, L_D decreases, resulting in stronger screening. Accordingly, the effect of the MPs decreases, and this turns out to be increased mobility as N_I increases. At high n (above $10^{19}cm^{-3}$), the mobility shows a weak T-dependence. In this region, μ_{II} still has noticeable T-dependence (see Fig. 3 (d) without DP), but μ_{Dip} has a very weak T-dependence (see Fig. 3 (e) where each scattering contribution is shown). Since the L_D is the function of electrons' average velocity and it depends on T, it embeds a strong T-dependence into μ_{II}. With the high n, however, the μ_{II} becomes less influential due to the more effective screening, and μ_{Dip} becomes the dominant term, producing the observed nearly T-independence mobility behavior.

IV. Conclusion

Our study shows that the disorder-induced MPs and DPs are critical ingredients in describing the transport of c-IGZO. Our analysis reveals that site disorders between Ga and Zn can play significant roles in the electron mobility of c-IGZO. Along with the wide applicability to various operating conditions, the present study provides a crucial understanding of the mobility behavior of the potential key material for future electronics and display applications.

References

[1] T. Kamiya and H. Hosono, "Material characteristics and applications of transparent amorphous oxide semiconductors," *NPG Asia Mater.*, vol. 2, no. 1, pp. 15–22, Jan. 2010, doi: 10.1038/asiamat.2010.5.

[2] K. Nomura, H. Ohta, A. Takagi, T. Kamiya, M. Hirano, and H. Hosono, "Room-temperature fabrication of transparent flexible thin-film transistors using amorphous oxide semiconductors," *Nature*, vol. 432, no. 7016, pp. 488–492, Nov. 2004, doi: 10.1038/nature03090.

[3] N. Kimizuka, and S. Yamazaki, *Physics and Technology of Crystalline Oxide Semiconductor CAAC-IGZO: Application to Displays*. Hoboken, NJ, USA: Wiley, 2017.

[4] S. Yamazaki, J. Koyama, Y. Yamamoto, and K. Okamoto, "15.1: Research, development, and application of crystalline oxide semiconductor," in *SID Symp. Dig. Tech. Papers*, vol. 43, no. 1, pp. 183–186, Jun. 2012, doi: 10.1002/j.2168-0159.2012.tb05742.x.

[5] Y. Kobayashi, D. Matsubayashi, S. Hondo, T. Yamamoto, Y. Okazaki, M. Nagai, S. Sasagawa, D. Ito, Y. Hata, T. Hamada, R. Arasawa, M. Sakakura, H. Suzawa, Y. Yamamoto, and S. Yamazaki, "Effect of surrounded-channel structure on electrical characteristics of *c*-axis aligned crystalline In–Ga–Zn–O field-effect transistor," *IEEE Electron Device Lett.*, vol. 36, no. 4, pp. 309–311, Apr. 2015, doi: 10.1109/LED.2015.2399911.

[6] T. Matsuzaki, H. Inoue, S. Nagatsuka, Y. Okazaki, T. Sasaki, K. Noda, Y. Sekine, D. Matsubayashi, T. Ishizu, T. Onuki, A. Isobe, Y. Shionoiri, K. Kato, J. Koyama, Y. Yamashita, and S. Yamazaki, "1Mb non-volatile random access memory using oxide semiconductor," in *Proc. 3rd IEEE Int. Memory Workshop (IMW)*, May 2011, pp. 185–188, doi: 10.1109/IMW.2011.5873242.

[7] D. M. Lynch, B. Zhu, B. D. A. Levin, D. A. Muller, D. G. Ast, R. G. Greene, and M. O. Thompson, "Characterization of reactively sputtered c-axis aligned nanocrystalline $InGaZnO_4$," *Appl. Phys. Lett.*, vol. 105, no. 26, Dec. 2014, Art. no. 262103, doi: 10.1063/1.4905208.

[8] M. Takahashi, M. Nakashima, T. Honda, A. Miyanaga, H. Ohara, T. Murakawa, M. Hayakawa, K. Akimoto, K. Okazaki, M. Yokoyama, M. Sakakura, and S. Yamazaki, "C-axis aligned crystalline In-Ga-Zn-oxide FET with high reliability," in *AM-FPD Dig.*, 2011, pp. 271–274.

[9] Y. Sekine, K. Furutani, Y. Shionoiri, K. Kato, J. Koyama, and S. Yamazaki, "Success in measurement the lowest off-state current of transistor in the world," *ECS Trans.*, vol. 37, pp. 77–88, Jun. 2011, doi: 10.1149/1.3600726.

[10] K. Nomura, T. Kamiya, H. Ohta, K. Ueda, M. Hirano, and H. Hosono, "Carrier transport in transparent oxide semiconductor with intrinsic structural randomness probed using single-crystalline $InGaO_3(ZnO)_5$ films," *Appl. Phys. Lett.*, vol. 85, no. 11, pp. 1993–1995, Sep. 2004, doi: 10.1063/1.1788897.

[11] T. Kamiya, K. Nomura, and H. Hosono, "Electronic structures above mobility edges in crystalline and amorphous In-Ga-Zn-O: Percolation conduction examined by analytical model," *J. Display Technol.*, vol. 5, no. 12, pp. 462–467, Dec. 2009, doi: 10.1109/JDT.2009.2022064.

[12] Y. Kang, Y. Cho, and S. Han, "Cation disorder as the major electron scattering source in crystalline InGaZnO," *Appl. Phys. Lett.*, vol. 102, no. 15, Apr. 2013, Art. no. 152104, doi: 10.1063/1.4802093.

[13] Y. Tanaka, K. Wada, Y. Kobayashi, T. Fujii, S. J. Denholme, R. Sekine, N. Kase, N. Kimizuka, and N. Miyakawa, "Single crystal growth of bulk InGaZnO4 and analysis of its intrinsic transport properties," *CrystEngComm*, vol. 21, no. 19, pp. 2985–2993, May 2019, doi: 10.1039/C9CE00007K.

[14] P. Giannozzi, S. Baroni, N. Bonini, M. Calandra, R. Car, C. Cavazzoni, D. Ceresoli, G. L. Chiarotti, M. Cococcioni, I. Dabo, A. D. Corso, S. de Gironcoli, S. Fabris, G. Fratesi, R. Gebauer, U. Gerstmann, C. Gougoussis, A. Kokalj, M. Lazzeri, L. Martin-Samos, N. Marzari, F. Mauri, R. Mazzarello, S. Paolini, A. Pasquarello, L. Paulatto, C. Sbraccia, S. Scandolo, G. Sclauzero, A. P. Seitsonen, A. Smogunov, P. Umari, and R. M. Wentzcovitch, "QUANTUM ESPRESSO: A modular and open-source software project for quantum simulations of materials," *J. Phys., Condens. Matter*, vol. 21, no. 39, Sep. 2009, Art. no. 395502, doi: 10.1088/0953-8984/21/39/395502.

[15] D. R. Hamann, "Optimized norm-conserving vanderbilt pseudopotentials," *Phys. Rev. B*, vol. 88, no. 8, Aug. 2013, Art. no. 085117, doi: 10.1103/PhysRevB.88.085117.

[16] B. K. Ridley, *Quantum Processes in Semiconductors*, 5rd ed. New York, NY, USA: Oxford Univ. Press, 2013.

[17] M. Lundstorm, *Fundamentals of Carrier Transport*. Cambridge, U.K.: Cambridge Univ. Press, 2000.

[18] S. Baroni, S. de Gironcoli, A. Dal Corso, and P. Giannozzi, "Phonons and related crystal properties from density-functional perturbation theory," *Rev. Modern Phys.*, vol. 73, no. 2, pp. 515–562, Jul. 2001, doi: 10.1103/RevModPhys.73.515.

[19] S. Matsuda, T. Hiramatsu, R. Honda, D. Matsubayashi, H. Tomisu, Y. Kobayashi, K. Tochibayashi, R. Hodo, H. Fujiki, Y. Yamamoto, M. Tsubuku, Y. Okazaki, and S. Yamazaki, "30-nm-channel-length c-axis aligned crystalline In-Ga-Zn-O transistors with low off-state leakage current and steep subthreshold characteristics," in *Proc. Symp. VLSI Technol. (VLSI Technol.)*, Jun. 2015, pp. 216–217, doi: 10.1109/VLSIT.2015.7223680.

[20] M. L. Cohen, and S. G. Louie, *Fundamentals of Condensed Matter Physics*. Cambridge, U.K.: Cambridge Univ. Press, 2016, pp. 220–224.